Contents lists available at ScienceDirect

Renewable Energy

journal homepage: http://ees.elsevier.com

Transposition of the mechanical behavior from model to prototype of Francis turbines

David Valentín [a,*], Alexandre Presas [a], Carme Valero [a], Mònica Egusquiza [a], Eduard Egusquiza [a], Joao Gomes [b], François Avellan [b]

[a] Center for Industrial Diagnostics and Fluid Dynamics (CDIF), Polytechnic University of Catalonia (UPC), Av. Diagonal, 647, ETSEIB, 08028, Barcelona, Spain
[b] EPFL Laboratory for Hydraulic Machines, Av. de Cour 33 Bis, 1007, Lausanne, Switzerland

ARTICLE INFO

Article history:
Received 10 January 2019
Accepted 23 January 2020
Available online xxx

Keywords
Hydropower
Transposition
Similitude
Stress
Francis runner

ABSTRACT

Hydropower is nowadays essential for balancing the electrical grid providing flexibility and fast response. The role of hydraulic turbines has changed from working at their Best Efficiency Point (BEP) to work in the whole operating range when demanded. Francis turbines working at off-design conditions suffer from dynamic problems that affect the useful life of their components, especially of the runner.Reduced scale physical models of Francis turbines are widely used to determine their hydraulic behavior. Most of the hydraulic parameters obtained in model tests are transposable to prototype by using the similarity theories as long as they meet similitude requirements. However, from the mechanical behavior point of view, both model and prototype structures are not always similar and the mechanical behavior of the model is often not considered for transposition.In this paper, a transposition method for the mechanical behavior of Francis turbines models is presented and the results are compared with the real size prototype. The modal behavior of the runner, its stress and fatigue life estimation for different operating conditions are experimentally compared for both model and prototype. Results present the possibilities and limitations of transposing the mechanical parameters from model to prototype.

1. Introduction

Francis turbines are one of the most used type of hydraulic turbines for electricity generation representing the 60% of the installed hydropower capacity in the world [1]. This type of turbines are usually designed to work in their Best Efficiency Point (BEP), which is defined for the rated values of head and discharge. However, they are able to operate in a wider range of head and discharge values while featuring lower performance. Nowadays, with the massive entrance of other renewables sources such as wind and solar power, hydraulic turbines are demanded to work in their whole operating range to provide fast response and regulation capacity to the electric power system [2–4].

When Francis turbines operate out of their BEP, they can experience dynamic problems related with part-load vortex rope [5–9], overload vortex rope [1,10], erosive cavitation [11,12], fatigue problems [13–15] as well as power swing [1,10,16]. The hydraulic excitations on the prototype and relevant parameters such as efficiency are generally well estimated by transposition of the experimental results obtained in reduced scale physical model tests [17]. Deep part load (discharge below 0.5 times the discharge at the BEP), part load (discharge between 0.5 and 0.9 times the discharge at the BEP) and overload regimes (over the discharge at the BEP) had been successfully reproduced in reduced scale models in the past [1,5–8,18,19] providing transposable results to the prototype. However, although these studies show generally a successful transposition of the hydraulic excitations, the possible extrapolation of structural response characteristics of the runner is much less analyzed.

In terms of modal behavior, model and prototype of Francis turbines exhibit rather different characteristics. From the theoretical point of view, the modal behavior can be transposed from model to prototype using similarity laws [20–23]. Therefore, natural frequencies, damping ratios and mode-shapes of the prototype should be possible to be transposed from the model test results. However, in practice, the damping ratio, which includes the structural damping and the fluid damping and which are not linear with the structural response [24], has been demonstrated to not be transposable [20] and, therefore, it has to be obtained experimentally [25–28]. Furthermore, the runner natural frequency values are different in air than in water [29,30] and they are also affected by the nearby rigid surfaces such as axial and radial gaps between the runner and casing [25,31,32], and by the rotation speed of the runner, especially in high head Francis and Pump-Turbine runners [33–35]. Non-rigid nearby surfaces [36] and acoustic natural frequencies of the surrounding water [37] could also have influence on the natural frequencies of the runner. The stiffness characteristics of the nearby surfaces to the runner can be rather different in model than in prototype, since head and lower covers are usually not manufactured following similarity laws, and either the stiffness of the model test rig support is not comparable to the one in a power

* Corresponding author.
E-mail address: david.valentin@upc.edu (D. Valentín)

https://doi.org/10.1016/j.renene.2020.01.115
0960-1481/

plant. Additionally, parameters that influence the acoustic natural frequencies of the surrounding water, such as the speed of sound inside the runner channels, could be different between both model and prototype. All this means, that the amplitude of vibration in or near resonance conditions is not transposable at all, but out of resonance conditions, the mechanical behavior could be similar.

The mechanical response of prototype Francis turbine runners under operation have been measured in the past using strain gauges installed in the runner blades [38–43]. Furthermore, it has been also obtained in reduced scale models [44,45]. In these cases, the stress in the runner blades was analyzed for different operating conditions and fatigue analyses could identify which regime was worse for the runner life-time. According to the results of those studies, different designs of Francis runners have different behavior in terms of life-time, and the worst operating condition is not always the same for the different designs. In addition, a transposition method from model to prototype of the stress behavior under different operating conditions has not been studied before for this kind of machines.

In this paper, a method to transpose the mechanical behavior of reduced scale models to prototypes is applied. To do so, a reduced scale model and its full size prototype are analyzed in detail from the mechanical point of view. The prototype case study is a medium-high head Francis turbine of 444 MW rated power and its reduced scale model (1:16 scale) is installed in the closed-loop PF3 test rig of the EPFL Laboratory for Hydraulic Machines. Experimental Modal Analysis (EMA) of both runners have been performed in air as well as strain measurements in the blades for the whole operating range of the turbine. After applying the similarity theories presented in the paper, results obtained for modal analysis and for stress under operation permit identifying the transposable operating points and parameters from model to prototype.

2. Similitude conditions

2.1. Hydraulic similitude

Reduced scale physical models of Francis turbines are designed and manufactured according to the IEC 60193 standard [17]. This standard defines the dimensionless numbers to use when transposing from model to prototype, but only from the point of view of hydraulic behavior. To achieve hydrodynamic similitude between two hydraulic turbines M and P (where M can stand for model and P for prototype) the following conditions should be met [17]:

- Geometrical similitude of water passages between machines M and P, including all the components, *i.e.* the spiral case, the stay vanes, the guide vanes, the runner and the draft tube.
- Kinematical similitude between two similar operating points of machines M and P, ensuring that the diagrams of the absolute flow velocity, the rotating velocity and the relative flow velocity forms two corresponding similar triangles.
- Dynamic similitude to ensure identical ratios of the various forces, acting between the fluid and the components of each machine. These ratios are defined by dimensionless terms and are identified by the fluid mechanics similarity numbers. The most important are listed in Table 1.

Table 1
Hydraulic similarity numbers.

Similarity number	Definition	Similarity number	Definition
Reynolds (Re)	$\frac{vL}{\nu}$	Weber (We)	$\frac{\rho L v^2}{\gamma}$
Euler (Eu)	$\frac{\Delta p}{\rho v^2}$	Strouhal (St)	$\frac{fL}{v}$
Froude (Fr)	$\frac{v}{\sqrt{gL}}$	Thoma (σ_{thoma})	$\frac{NPSE}{E}$

Usually, it is impossible to choose the test conditions to satisfy the various similarity numbers simultaneously. Therefore, the similarity condition to be considered should be the one with the greatest influence on the results. For hydraulic machinery it is agreed that, apart from the geometrical similarity between M and P, the ratios of corresponding flow velocity components at any homologous point of both machines should be identical, making the corresponding velocity triangles at the runner geometrically similar. As a consequence, both machines have to fulfil one of the following requirements at corresponding operating points:

- Identical discharge (Q_{nD}), energy (E_{nD}) and cavitation coefficients (σ_{nD})

  or

- Identical discharge (Q_{ED}) and speed (n_{ED}) factors and Thoma number (σ)

In the present paper, the second requirement is the one imposed and the definition of the involved dimensionless numbers is show in Table 2. Other dimensionless parameters derived from the ones presented in Table 2 are also commonly used when transposing results of pressure and force from model to prototype. These parameters are listed in Table 3.

Therefore, the net head ($H_n = E/g$) of the model is reflected in the speed factor (n_{ED}) as well as in the discharge factor (Q_{ED}), while the discharge (Q) is only included in the last. The discharge has to be smaller in the model than in the prototype, to maintain the corresponding velocity triangles in the model and in the prototype, the rotating speed (n) of the model has to be larger than in the prototype. In that way, all the hydraulic phenomena related with the rotating speed (n), such as Rotor Stator Interaction (RSI) [46,47] or Vortex Rope (VR) [5–7] happens at higher frequencies in the model than in the prototype. Hence, the hydraulic phenomena frequencies (f_{hyd}) are agreed [17] to be dimensionless using the rotating speed (n). In that way, the frequency used to transpose the hydraulic results from model to prototype is the called reduced frequency (f_r) (see Eq. (1)).

$$f_r = \frac{f_{hid}}{n} \tag{1}$$

The frequencies of the RSI phenomenon are dependent on the number of blades of the runner (z_b) and on the number of guide vanes (z_v) of the Francis turbine [48]. From the stationary frame, the RSI frequencies are given by Eq. (2), where $i = 1, 2, 3 \ldots, \infty$ and, from the rotating frame, the RSI frequencies are obtained with Eq. (3), where again

Table 2
Main dimensionless parameters for hydraulic similarity.

Term	Symbol	Definition
Speed factor	n_{ED}	$\frac{nD}{E^{0.5}}$
Discharge factor	Q_{ED}	$\frac{Q}{D^2 E^{0.5}}$

Table 3
Derived dimensionless parameters for hydraulic transposition.

Term	Symbol	Definition
Pressure coefficient	C_P	$\frac{\Delta p}{\rho \frac{E}{F}}$
Force factor	F_{ED}	$\frac{F}{\rho D^2 E}$

j = 1, 2, 3 …, ∞. The shape of the excitation ($k_{i,j}$) at every frequency (f_b or f_v) is given by the combination of i times z_b and j times z_v (see Eq. (4)). The sign of $k_{i,j}$ means that the pressure waves are travelling in the opposite (negative sign) or in the same direction (positive sign) that the rotating speed.

$$f_{b,i} = i \times n \times z_b \tag{2}$$

$$f_{v,j} = j \times n \times z_v \tag{3}$$

$$k_{i,j} = i \times z_b - j \times z_v \tag{4}$$

To transpose RSI frequencies from model to prototype, the reduced frequency (f_r) parameter has to be used (Eq. (1)), hence Eqs. (2) and (3) can be rewritten as in Eqs. (5) and (6).

$$f_{rb,i} = i \times Z_b \tag{5}$$

$$f_{rv,j} = j \times Z_v \tag{6}$$

The VR frequency is usually found at 0.25 ÷ 0.40 times the rotating frequency from the stationary side ($f_{rVR,stat} = 0.25 \sim 0.4$) [11,49] and therefore at 0.60 ÷ 0.75 times the rotating frequency from the rotating point of view ($f_{rVR,rot} = 0.60 \sim 0.75$)

This means that the main hydraulic excitation frequencies in Francis turbines are scalable from model to prototype by only the rotating speed.

2.2. Mechanical similarity

From the mechanical point of view, the similarity laws have been studied since many years [20–22]. Similarity laws are used for both free and forced responses in structural dynamics analysis. They are based on the conservation between model and prototype of three basic mechanics laws: the Hooke's, the Newton's second law and the internal friction law. The dimensionless numbers defined by those laws are shown in Table 4.

2.2.1. Modal behavior scaling

The modal behavior of structures refers to the dynamic response of a structure under free vibration response, which can be defined by their natural frequencies, mode-shapes and damping ratios (Eq. (7)).

$$[M]\{\ddot{u}\} + [C]\{\dot{u}\} + [K]\{u\} = 0 \tag{7}$$

As in the case of the hydraulic similarity, it is difficult to ensure the complete similarity by conserving all the three dimensionless numbers presented in Table 4. For this, relaxation methods such as disregarding the weak laws are used. In most of vibrating structures, gravity exerts insignificant influence on the terms of Eq. (7) and therefore is neglected. With this assumption and by the conservation of the dimensionless numbers presented in Table 4, the similarity laws to be used when transposing the modal behavior of structures are presented in Table 5. In this table, λ is used as the definition of scale, being its subscript the variable of the scale. For example, λ_L is the geometric scale, defined as $\lambda_L = \frac{L_P}{L_M}$.

Table 4
Governing laws and dimensionless numbers for mechanical similarity.

Governing law	Formula	Dimensionless number
Hooke's law	$\sigma = Y\varepsilon$	$\pi_1 = \frac{F}{L^2 Y \varepsilon}$
Newton's second law	$dF = dma$	$\pi_2 = \frac{Ft^2}{\rho L^4}$
Internal friction law	$dU = dV\beta\sigma_m^3$	$\pi_3 = \frac{F\sqrt{\beta}}{L^2}$

Table 5
Mechanical similarity laws for modal behavior.

Similarity law	Formula	Similarity law	Formula
Modal mass scale	$\lambda_m = \lambda_L^3 \lambda_\rho$	Frequency scale	$\lambda_\omega = \frac{1}{\lambda_L}\sqrt{\frac{\lambda_\rho}{\lambda_Y}}$
Modal damping scale	$\lambda_c = \lambda_L^2 \sqrt{\lambda_\rho \lambda_Y}$	Damping ratio scale	$\lambda_\xi = 1$
Modal stiffness scale	$\lambda_k = \lambda_L \lambda_Y$	Mode shape scale	$\lambda_\psi = 1$

Therefore, according to the similarity laws presented in Table 5, natural frequencies are scalable from model to prototype by using the geometric scale (λ_L), the density (λ_ρ) and Young modulus scale (λ_Y). For the same material between model and prototype, something usual in the case of Francis turbines, the natural frequencies are λ_l times smaller in prototype than in the model. Furthermore, the mode-shapes are exactly the same in both model and prototypes, while in theory the damping ratio should be also the same. However, in practice, as said in the introduction section, it is usually not transposable because it is a non-linear parameter that strongly depend on the boundary conditions and other parameters difficult to maintain from model to prototype [20].

2.2.2. Forced response scaling

The forced response of a structure can be understood as the displacement, velocity or acceleration of the structural field, when a force $F(t)$ is applied on it (Eq. (8)).

$$[M]\{\ddot{u}\} + [C]\{\dot{u}\} + [K]\{u\} = \{F(t)\} \tag{8}$$

Applying the conservation of the laws in Table 4, the scaling formulas for the most important parameters when analyzing forced response cases can be obtained (Table 6 [21]). The same relaxation factors than for the case of the modal behavior have been used. It is seen that the force should be scaled between model and prototype by using the geometric scale and the Young modulus scale, whilst the stress should be only scaled by the young modulus scale. This means that for the same material for model and prototype, the scale factor of the stress will be 1, and the force is λ_l^2 times higher in the prototype than in the model.

In the case of Francis turbines, the force is given by the hydraulic excitation and according to the hydraulic similarity laws, the force factor (F_{ED}) or the pressure coefficient (C_P) have to be used to transpose forces and pressures from model to prototype (see Table 3). Eq. (9) shows the hydraulic pressure coefficient scale derived from the pressure coefficient (C_P) shown in Table 3. This scale is dependent on the force scale, the water density scale, the geometric scale and the specific energy scale. Isolating the force scale from Eq. (9), the similarity law for the hydraulic force is obtained (Eq. (10)). One can see that the mechanical similarity law of the force (Table 6) and the hydraulic similarity law for the force (Eq. (10)) cannot be met at the same time when considering the same structural material for the runner in model and prototype.

Table 6
Mechanical similarity laws for forced response.

Similarity law	Formula
Time scale	$\lambda_t = \lambda_l \sqrt{\frac{\lambda_\rho}{\lambda_Y}}$
Stress scale	$\lambda_\sigma = \lambda_Y$
Force scale	$\lambda_F = \lambda_l^2 \lambda_Y$
Acceleration scale	$\lambda_a = \frac{\lambda_l \lambda_\rho}{\lambda_Y}$

$$\lambda_{C_p} = \frac{\lambda_P}{\lambda_E \lambda_{\rho_{water}}} = \frac{\lambda_F}{\lambda_L^2 \lambda_E \lambda_{\rho_{water}}} \tag{9}$$

$$\lambda_F = \lambda_{C_p} \lambda_L^2 \lambda_E \lambda_{\rho_{water}} \tag{10}$$

To overcome this problem, the similarity law for the hydraulic force is imposed in the mechanical similarity model considering that the stress in the structure is a consequence of the force applied to it. In that way, a stress/force coefficient can be introduced (Eq. (11)) to be the one that has to be conserved.

$$\frac{\lambda_\sigma}{\lambda_F} = \frac{\lambda_Y}{\lambda_L^2 \lambda_Y} = \frac{1}{\lambda_L^2} \tag{11}$$

Imposing the hydraulic force scale (Eq. (10)) into Eq. (11), and considering the water density scale as 1, the new stress scale found is shown in Eq. (12). This means that the stress can be scaled from model to prototype by the specific energy scale λ_E and the pressure coefficient scale λ_{CP}.

$$\lambda_\sigma = \frac{\lambda_F}{\lambda_L^2} = \lambda_{C_p} \lambda_E \tag{12}$$

It should also be noted that if the hydraulic force coincides in frequency and in shape with a natural frequency and mode-shape of the runner [47], resonance occurs and the amplitude of vibration as well as stress in the structure are amplified. The main hydraulic excitation that can produce this kind of phenomenon in Francis turbines is the RSI. However, resonance may occur in the model and not in the prototype or vice versa. The reason is that the RSI is represented in a dimensionless way by the reduced frequency (f_r) (Eq. (1)) which is dependent on the rotating speed. The natural frequency is represented in a dimensionless way by the frequency scale (λ_ω) (Table 5) which is dependent on the geometric scale when the material of both model and prototype is the same. Hence, to have the same kind of resonances in both model and prototype runners made of the same material, the rotating speed scale should be the same as the geometric scale. This cannot happen since according to the n_{ED} and Q_{ED} factors, rotating speed and geometric scales are dependently related. Therefore, in case of resonance, the mechanical behavior from model to prototype is not transposable.

3. Case study

3.1. Prototype

The prototype to study in this paper is a large medium-head Francis turbine. This Francis Turbine features a rated power of 444 MW and a rated head of 170 m. The study of the dynamic behavior of this Francis Turbine is part of the collaborative European Project Hyperbole (FP7-ENERGY-2013-1) [50]. The runner has 16 blades ($Z_b = 16$), whereas the distributor has 20 guide vanes ($z_v = 20$). The rotating speed of the machine is 128.6 min^{-1} (2.14 Hz) and its outlet diameter is $D = 5.4$ m. Taking advantage of an overhaul in the power plant, the machine was accessible to install several sensors in the rotating parts and in the stationary parts. A large number of sensors were used to detect a large number of dynamic phenomena occurring in this generating unit, such as power sings, hydraulic and mechanical resonance.

3.1.1. Instrumentation

The runner was instrumented with 24 strain gauges and eight pressure sensors located in two different blades. Apart from the onboard instrumentation, different sensors were also located all along the stationary parts of the machine. Pressure sensors were located in penstock, spiral case and draft tube, accelerometers were placed in the bearings, head cover and guide vanes, displacement probes were also installed in the bearings to measure the shaft vibration. Mechanical torque and electrical parameters such as current, voltage and generating power were also measured simultaneously. The operating conditions signals of guide vane opening and gross head were also measured. Detailed information about the sensors position and their characteristics can be found in Refs. [10,51–53].

3.1.2. Procedure

First, an EMA (Experimental Modal Analysis) was performed impacting the runner in 32 different points and measuring its response with accelerometers and strain gauges (see Ref. [51] for further information about these tests). The runner was impacted radially in 16 positions of the band outlet (in the middle of every runner channel) and also radially in every blade (another 16 positions). For every point of impact, five different impacts were undertaken in order to compute the average of those impacts when analyzing. Accelerometers were not moved during the tests, only the impact position was changed. This method is called the roving hammer method.

Once the EMA was finished, the experimental tests while in operation started. These tests were performed for the different operating conditions of the machine. The net head remained constant during the tests, which at that time was 1.06 times the rated net head for that machine. Different ramp-up and ramp-downs of power were performed, as well as, operation in fixed powers. For this paper, the operating conditions selected to analyze were the ones where the machine was operating at steady conditions with fixed guide vane opening.

3.2. Reduced scale physical model set-up

The homologous reduced scale (1:16) physical model of the turbine prototype features a runner with $D = 0.35$ m outlet diameter and is installed in the closed-loop PF3 test rig of the EPFL Laboratory for Hydraulic Machines illustrated in Fig. 1. This test rig features two 400 kW axial pumps that can supply a maximum head of 100 m. The rotating speed of the runner can be changed to be adapted to the head conditions. The geometric scale of the runner is strictly followed for the hydraulic part of the runner, i.e. the water passages are exactly the same but scaled 1:16 from prototype. However, the runner structure is not exactly the same. As it can be seen in Fig. 2, the crown in the model is thicker, which makes stiffer this part. The material of both prototype and model is stainless steel.

The modal analysis of the runner was performed in the Center for Industrial Diagnostics and Fluid Dynamics (CDIF) laboratory with the runner hung in the air as well as attached to a fixed boundary by its coupling with the shaft.

3.2.1. Instrumentation

As in the case of the prototype, the runner was instrumented with strain gauges. In this case eight strain gauges were installed in the suction side of the blade 9, eight more in the pressure side of the blade 13, and other four strain gauges in the pressure side and section side of blade 5 (total of 8) (see Fig. 3). To install the strain gauges with their cables, the blade surface was modified to allocate the instrumentation (see Fig. 3). The relative position of the strain gauges in the blade is slightly different in the model than in the prototype, being closer to the fillet radius in the case of the prototype. The nomenclature for those strain gauges is also shown in Fig. 3. The strain gauges used had a gauge factor of 163, and a sensitivity of 6.9 μm/m/V. After gluing the strain gauges in the runner, they were covered with a special epoxy resin to protect them from the water.

For the modal testing, three accelerometers (Dytran 3006A, 100 mV/g, 50g of weight) were located in the outlet of the runner at the band in the same angular position that the instrumented blades. The crown, blades and the band were impacted with an instru-

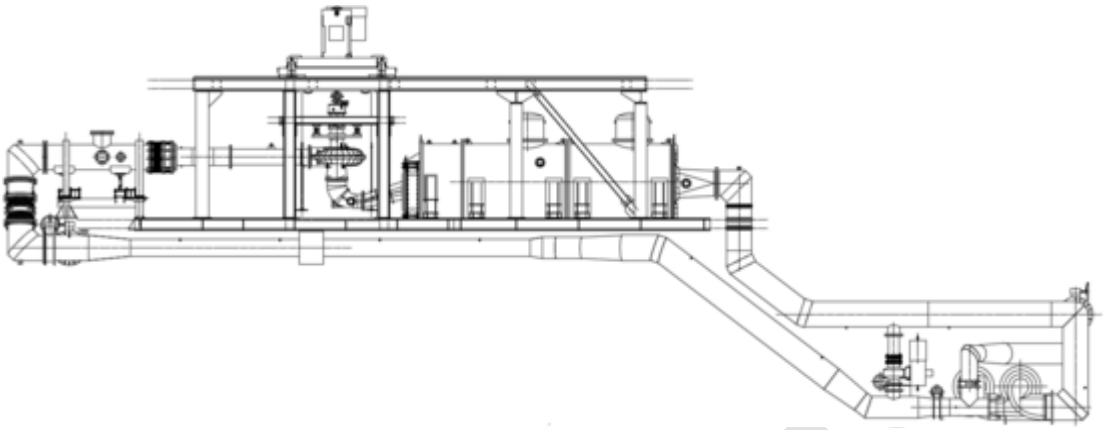

Fig. 1. Closed-loop test rig number 3 of the EPFL Laboratory for Hydraulic Machines.

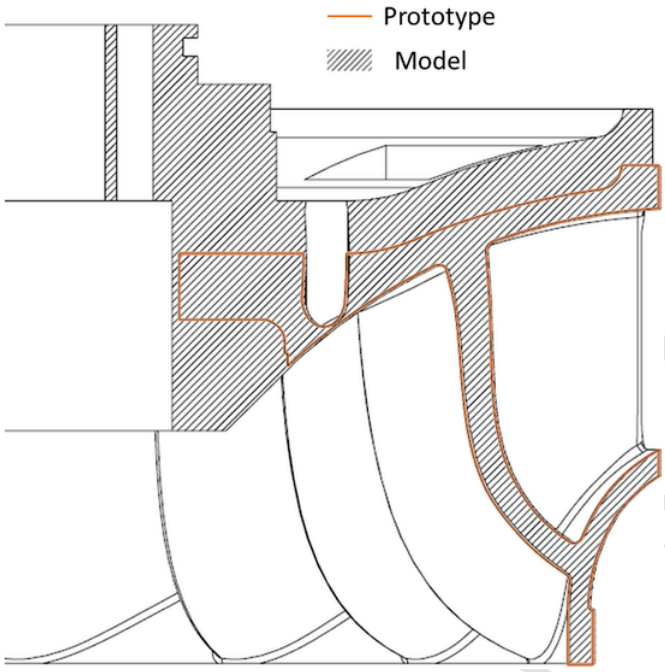

Fig. 2. Runner cross section. Comparison prototype and model.

mented hammer (Kistler 9722, 2.25 mV/N) as in the case of the prototype performing a roving hammer method. All the signals were acquired with an acquisition system (Brüel&Kjær Type 3053-B-120).

For the tests of the Francis turbine model during operation, different pressure sensors were also installed in the pipes, spiral casing and guide vanes. The output power and the operating conditions such as guide vane opening, head and discharge were also measured simultaneously.

3.2.2. Procedure

As in the case of the prototype, an EMA of the model runner was also performed. The runner was fixed by its coupling to the shaft and impacted in different positions. The runner was impacted in 48 different points (16 in band outlet, 16 in the blades and 16 in the crown). The Frequency Response Function (FRF) between the accelerometers and the hammer was computed and therefore the Operational Deflection Shape (ODS) of the runner was obtained. The natural frequencies, mode-shapes and damping ratios were extracted using the Complex Mode Indication Function (CMIF) with the Pulse Reflex commercial software [54].

The tests under operation were performed in the same n_{ED} = 0.277 and σ_{thoma} conditions than in the prototype and for the whole operating range (various Q_{ED}). This means that the rotating speed of the model was fixed at 769.5 min^{-1}. All the measurements are performed according to the IEC Standard [17].

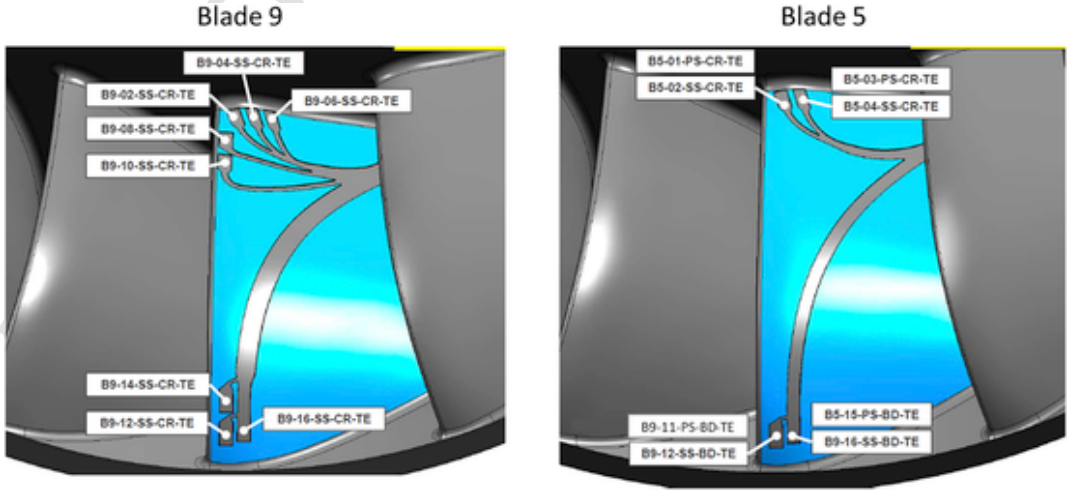

Fig. 3. Strain gauges location in the model.

4. Results

4.1. Modal behavior transposition

The results for the natural frequencies, mode-shapes and damping ratios for both model and prototype runners in air are listed in Table 7. The prototype results were already published in Ref. [51]. The mode-shapes are classified according to the number of nodal diameter (0ND, 1ND, …, 6ND), if they are global (G) (same deformation in crown, band and blades), blade dominant (BlD) (more deformation in blades) or crown dominant (CD) (more defamation in the crown). The ODS of the mode-shapes of both model and prototype can be observed in Fig. 4. It is evidenced that the mode-shapes are the same in both cases as theoretically is predicted in Table 5.

The transposed natural frequency values from the model to the prototype scale, $f_{n,trans}$, are calculated using the similarity laws of Table 5 and presented in Table 7. The error between the transposed and the measured frequency is also shown in the same table $\left(Error\,(\%) = 100\ \left(f_{n,trans} - f_{n,P}\right) / \left(f_{n,P}\right)\right)$. It is seen that the error is below 7% for almost all the modes except for the two first global modes (2ND, 3ND) and the ninth mode (0ND). In those modes there is an important deformation of the crown, while in the rest the deformation is mainly in the blades. The crown in the model is thicker (see Fig. 2) and therefore stiffer than in the prototype, this is why those modes are transposed with higher error. Besides, as said in the introduction section, the damping ratios are not transposable from model to prototype. According to theory (Table 5), damping ratios should be the same in both model and prototype, but results show rather higher values in the prototype than in the model. This behavior confirm the results presented before by Ref. [20].

4.2. Mechanical transposition under operation

4.2.1. Stress results for the whole operating range

For the transposition of the mechanical stress, different operating conditions in the whole operating range of both model and prototype were analyzed. Fig. 5 shows the mean and peak-to-peak values of the mechanical stresses obtained with three different strain gauges located in similar location in model and prototype. The maximum static stress (mean value) as well as the maximum dynamic stress (peak-to-peak values) are found in the pressure side near the crown for mainly all the operating conditions. The static stress is increasing when increasing Q_{ED} especially near the crown and they are rather constant or even decreasing in the band side. This behavior is directly related to the static pressure in the blade channel. However, the dynamic stress follows a different trend. There are clearly three different zones where the dynamic stress is affected. The first zone is corresponding to low part load operation ($Q_{ED} = 0.05 \div 0.12$), the second to high part load operation ($Q_{ED} = 0.12 \div 0.2$) and the third to overload operation ($Q_{ED} > 0.25$). These three zones can be identified at the same Q_{ED} in both model and prototype. The dynamic stress increases considerably at high part load operation ($Q_{ED} = 0.12 \div 0.2$), especially in the pressure side near the crown and in the prototype. The BEP in this machine is located at about $Q_{ED} = 0.2$ for the n_{ED} of the tests.

In Francis turbines, the vortex rope phenomenon appears at part load and sometimes at full load operation at frequencies below the runner rotating frequency. This phenomenon sometimes coincides for a certain Q_{ED} with a hydraulic natural frequency of the draft tube, spiral casing and penstock and it is amplified considerably [5,10]. To see if this is happening in the studied machine, a FFT has been applied to the time signal of the strain gauges for all the operating conditions of both model and prototype. Results are observed in Fig. 6. The frequency has been normalized with the rotating frequency, so the reduced frequency (f_r) is shown. Two plots from 0 to 1 of reduced frequency for both model and prototype are shown in order to see the low frequency phenomena related with the VR. Furthermore, two other plots from 1 to 80 of reduced frequency are also included to see the frequencies related with the RSI.

For the low part load operation ($Q_{ED} = 0.05 \div 0.12$), the same behavior in both model and prototype is obtained when looking at the low frequency phenomena. VR is detected from 0.6 to 0.75 times the rotating frequency with a resonance at about $Q_{ED} = 0.12$. For the full load operation ($Q_{ED} > 0.25$), an overload VR is detected in both model and prototype but at a slightly lower reduced frequency in the model than in the prototype. For the high part load operation ($Q_{ED} = 0.12 \div 0.2$), no low frequency phenomenon is observed, but the peak-to-peak values in these operating conditions are high (Fig. 5). The reason for that lies in the high frequency range (1–80 reduced frequency). The first three blade passing frequencies $\left(f_{rv,1} = z_v = 20\ ;\ f_{rv,2} = 2 \times z_v = 40;\ f_{rv,3} = 3 \times z_v = 60\right)$ are highlighted with a red dotted line in the plots (Fig. 6). It is seen that the stress amplitude in the first blade passing frequency ($f_{rb,1} = 20$) remains almost constant for all the operating range, but the second and the third ($f_{rb,2} = 40$, $f_{rb,3} = 60$) increase from $Q_{ED} = 0.15 \div 0.2$. This behavior is happening in both model and prototype. This means that the RSI is changing its characteristics at these points, which can be related to inlet cavitation modifying the pressure fluctuation in the runner inlet [55].

In the case of the prototype, the amplitude of the third blade passing frequency ($f_{rv,3} = 60$) is relatively higher than in the model. This

Table 7
Natural frequencies, mode-shapes and damping ratios for prototype, model and transposition from model to prototype.

Mode-Shape Number	Mode-Shape Name	Model		Prototype		Transposition	
		f_n [Hz]	ξ [%]	f_n [Hz]	ξ [%]	$f_{n,trans}$ [Hz]	Error [%]
1	**2ND-G**	1024.39	0.0838	46.44	1.0272	64.02	37.86
2	**3ND-G**	1780.75	0.0657	98.24	0.5498	111.30	13.29
3	**1ND-G**	1924.80	0.1026	129.14	2.4669	120.30	−6.85
4	**4ND-G**	2537.76	0.0370	148.08	0.3094	158.61	7.11
5	**2ND-BlD**	2625.11	0.0966	155.58	0.3469	164.07	5.46
6	**5ND-BlD**	2995.24	0.0584	181.03	0.2713	187.20	3.41
7	**3ND-BlD**	3188.22	0.0345	192.48	0.2394	199.26	3.52
8	**6ND-BlD**	3246.20	0.0353	197.89	0.2894	202.89	2.53
9	**0ND-BlD**	2818.15	0.0840	206.85	0.249	176.13	−14.85
10	**1ND-BlD**	3293.35	0.0160	209.38	0.2413	205.83	−1.69
11	**1ND-BlD**	3420.03	0.0095	216.99	0.8927	213.75	−1.49
12	**4ND-CD**	3932.59	0.0295	233.25	0.255	245.79	5.37

Mode-shape		Prototype	Model	Mode-shape		Prototype	Model
1	2ND-G-IPh	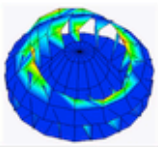	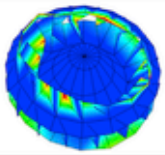	7	3ND-BlD-IPh	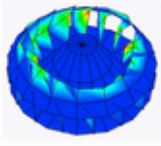	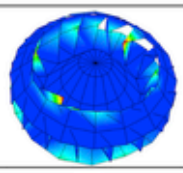
2	3ND-G-IPh	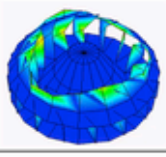	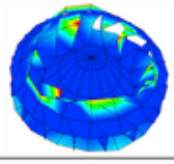	8	6ND-BlD-CPh	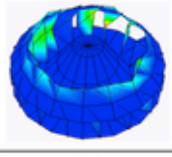	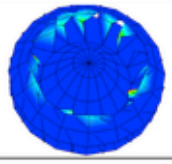
3	1ND-G-IPh	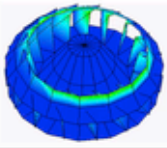	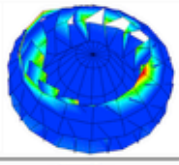	9	0ND-BlD-IPh	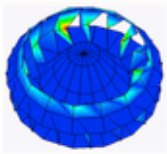	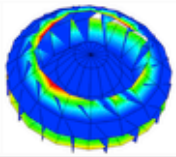
4	4ND-G-CPh	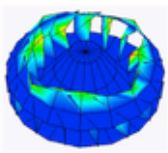	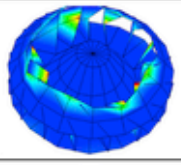	10	1ND-BlD-CPh	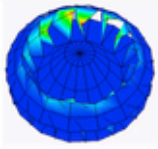	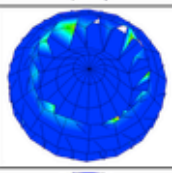
5	2ND-BlD-IPh	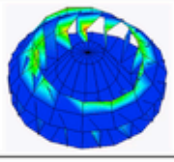	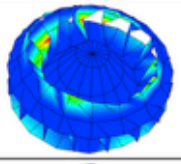	11	1ND-BlD-IPh	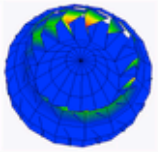	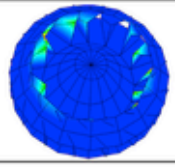
6	5ND-BlD-CPh	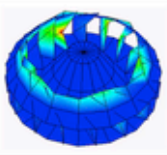	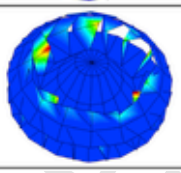	12	4ND-CD-IPh	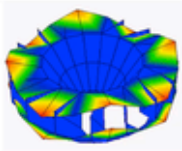	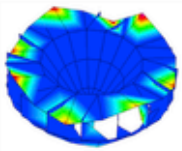

Fig. 4. Mode-shapes for model and prototype.

is because this excitation frequency coincides in shape and in frequency with a natural frequency of the runner. According to some studies [23,29,30,42], the natural frequencies can be reduced 50–60% when the runner is in operation in comparison with the runner in air, which makes the twelfth mode-shape (see Table 7 and Ref. [42]) excitable by the third blade passing frequency ($f_{v,3_P} = \frac{3 \cdot 128.6 \cdot 20}{60} = 128.6\ Hz$). In the model the natural frequencies are rather higher than the excitation frequency even considering the 50%–60% of frequency reduction due to the operation in water. The twelfth can be reduced up to 1900 Hz–2000 Hz (Table 7) but the excitation frequency is considerably smaller ($f_{v,3_M} = \frac{3 \cdot 769.5 \cdot 20}{60} = 769.5\ Hz$). In this case, the dynamic stress cannot be transposable at all as commented in section 2.2.2.

4.2.2. Stress transposition

As commented in section 2.2.2, to transpose the stress behavior from model to prototype, the relationship between stress and force should be used. This relationship is defined by the specific energy scale and the *Cp* scale (Eq. (12)). *Cp* values for this case for model and prototype are plotted in Fig. 7. In this figure, the peak-to-peak values filtered at frequencies below the rotating frequency and in the whole frequency range are shown for the pressure sensors located in the draft tube and in the penstock. It is seen that the C_P of the prototype is very well predicted by the model in all of the operating points but in the part load resonance ($Q_{ED} = 0.14$) it is slightly under estimated. Therefore, the *Cp* scale (λ_{CP}) is 1 for almost all of the operating conditions and from now on, it will be considered as this for all the operating range. This means that the relationship stress/specific energy is the one that should be conserved between model and prototype in this case.

The results for the relationship stress and specific energy (σ/E) for both model and prototype are shown in Fig. 8. Mean values, overall peak-to-peak values and filtered peak-to-peak values below the rotating frequency are observed in this figure. It is seen that the trends of model and prototype are almost the same for all the strain gauges but with a constant offset of almost two times smaller the model than the prototype. This difference is not due to the difference in pressure amplitude between model and prototype since the C_P values are rather similar in both cases (Fig. 7). The main reasons for this offset behavior could be that the strain gauges are not in the same relative position in the blade between model and prototype and that the crown is thicker in the model (see Fig. 2). The strain gauges in the prototype are closer to the blades fillets, where the maximum stress is normally concentrated, therefore higher values of σ/E are expected in the prototype than in the model. In addition, according to numerical simulations, a thicker crown makes the structure stiffer and therefore more difficult to be deformed, expecting also higher σ/E values in the prototype than in the model.

Nevertheless, the amplitude of the strain gauges due to the position and crown thickness could be corrected by using numerical FEM (Finite Element Method) simulations. However, the relative amplitudes between operating conditions are very well predicted with the model.

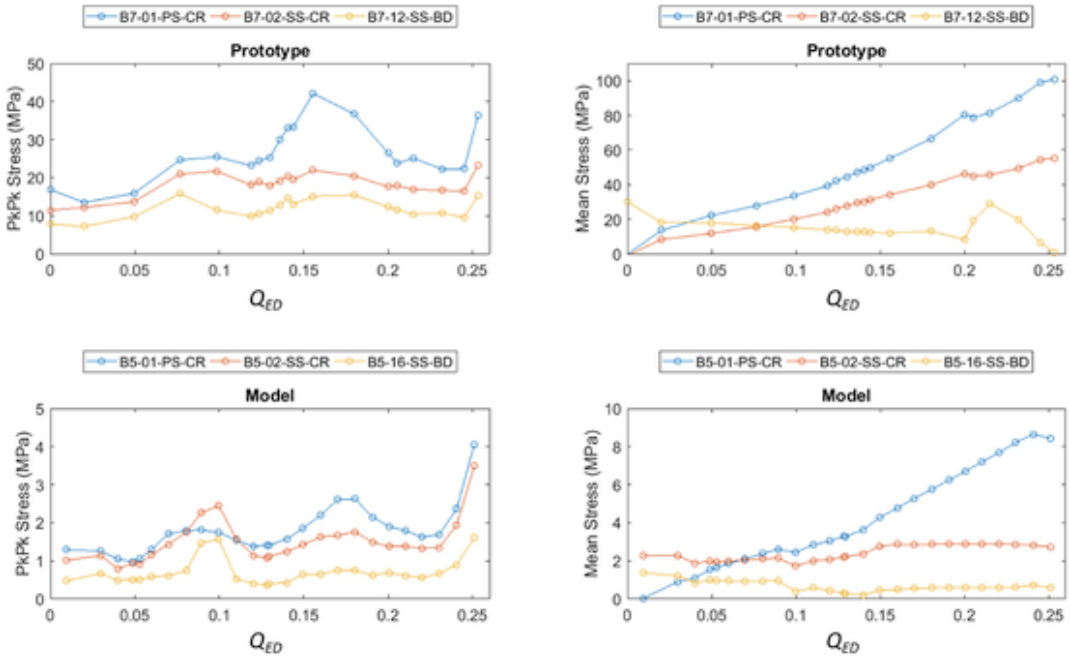

Fig. 5. Peak-to-peak and mean values of mechanical stress for the whole operating range.

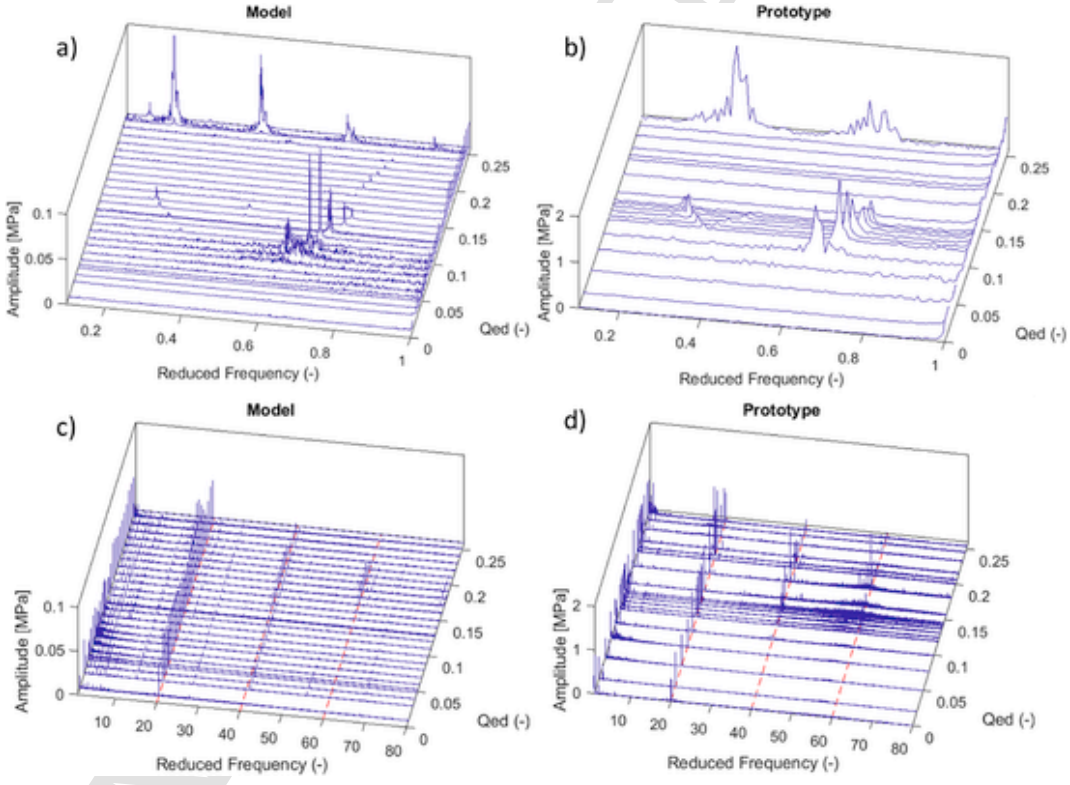

Fig. 6. FFT Waterfall plots for the whole operating range of both model and prototype. a) B5-01-PS-CR (Model) from 0 to 1 of reduced frequency. b) B7-01-PS-CR (Prototype) from 0 to 1 of reduced frequency. c) B5-01-PS-CR (Model) from 1 to 80 of reduced frequency. d) B7-01-PS-CR (Prototype) from 1 to 80 of reduced frequency. a) B5-01-PS-CR (Model) from 0 to 1 of reduced frequency. b) B7-01-PS-CR (Prototype) from 0 to 1 of reduced frequency.

4.2.3. Fatigue life-time transposition

With the stress results obtained with the strain gauges, a fatigue analysis can be performed to estimate the number of cycles to fatigue of the structure. To do so, a rainflow counting algorithm [56] is used with the time signal of the strain gauge. This algorithm is based on the idea of the cumulative damage. This means that the damage caused by the different excitations due to different frequencies and amplitudes can be summed to obtain the total damage. To be able to compare model and prototype damages, the stress time signal from the model strain gauges should be transposed to prototype scale by using the reduced frequency relationship. The stress amplitudes are lower in

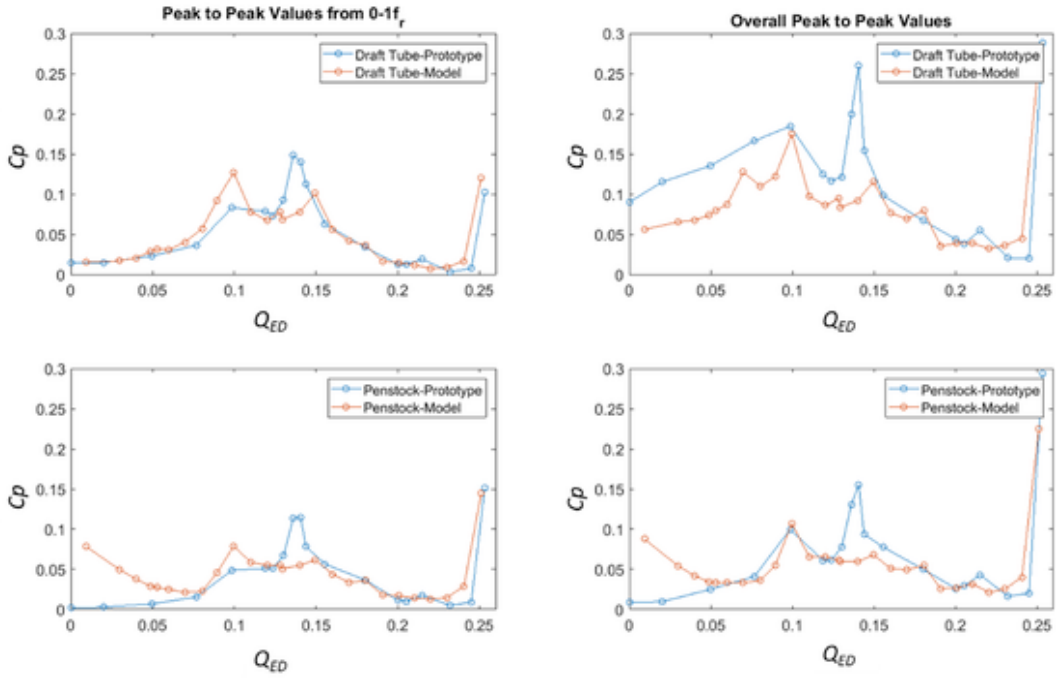

Fig. 7. Cp peak-to-peak values in the draft tube (upside) and in the penstock (downside) for both model (orange) and prototype (blue). On the left filtered values from 0 to 1 reduced frequency, on the right overall peak to peak values. (For interpretation of the references to colour in this figure legend, the reader is referred to the Web version of this article.)

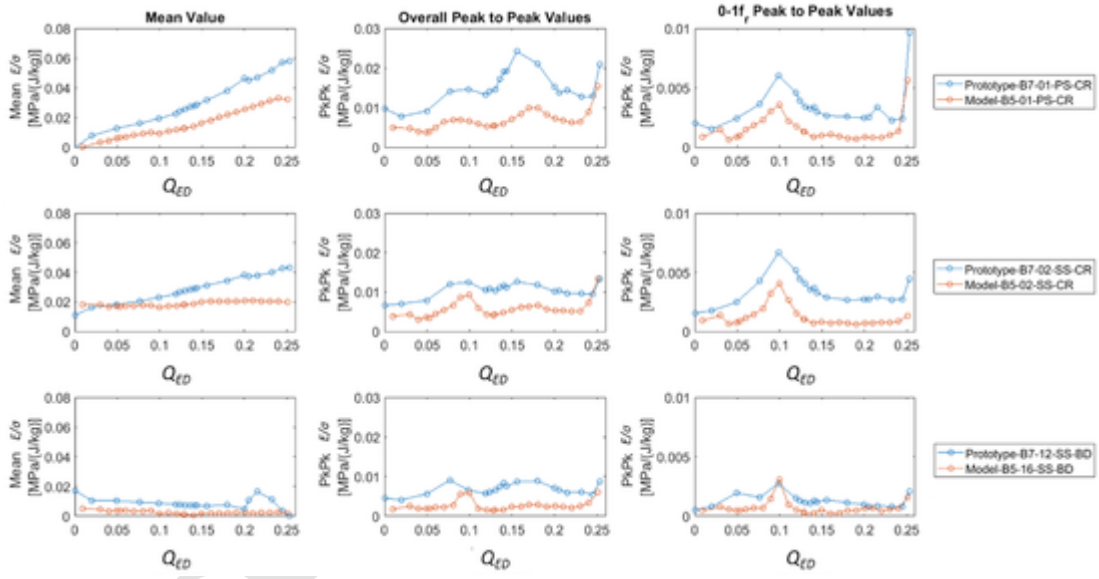

Fig. 8. Comparison of σ/E between model and prototype for three different strain gauges and the whole operating range.

model than in prototype but with a constant relationship between different operating conditions (see Fig. 8), hence the relative damage between operating conditions can be compared in both cases. The relative damage in this case is defined with the damage in every operating condition divided by the damage at the BEP.

Fig. 9 shows the results of the relative damage for the different operating conditions and positions in the blade. The relative damage is normalized with respect to the damage at the BEP and to the strain gauge in the pressure side near the crown, which is where the stress is maximum for this runner. It is seen that the worst situation for this runner is in the full load condition (Q_{ED} = 0.252). However, the fatigue damage in the range of the high part load operation (Q_{ED} = 0.12 ÷ 0.2) is also important in this runner. In the prototype, this value is higher than in the model because there is an excitation of a natural frequency of the runner at these conditions (explained in section 4.2) and in the model there is not. However, the hydraulic excitation is still existing in the model and therefore the damage at those conditions is also high. In comparison with the other operating conditions, this one is much worse in terms of fatigue since it is at higher frequency, which produces much more cycles per second than the low frequency excitations (VR) predominant in the rest of the operating points.

The mechanical behavior of this machine is not common since in the BEP the stress distribution is higher than in low part load operation. Usually, the part load operation in Francis turbines is worse in terms of fatigue than in the BEP [39,43]. Nevertheless, this behav-

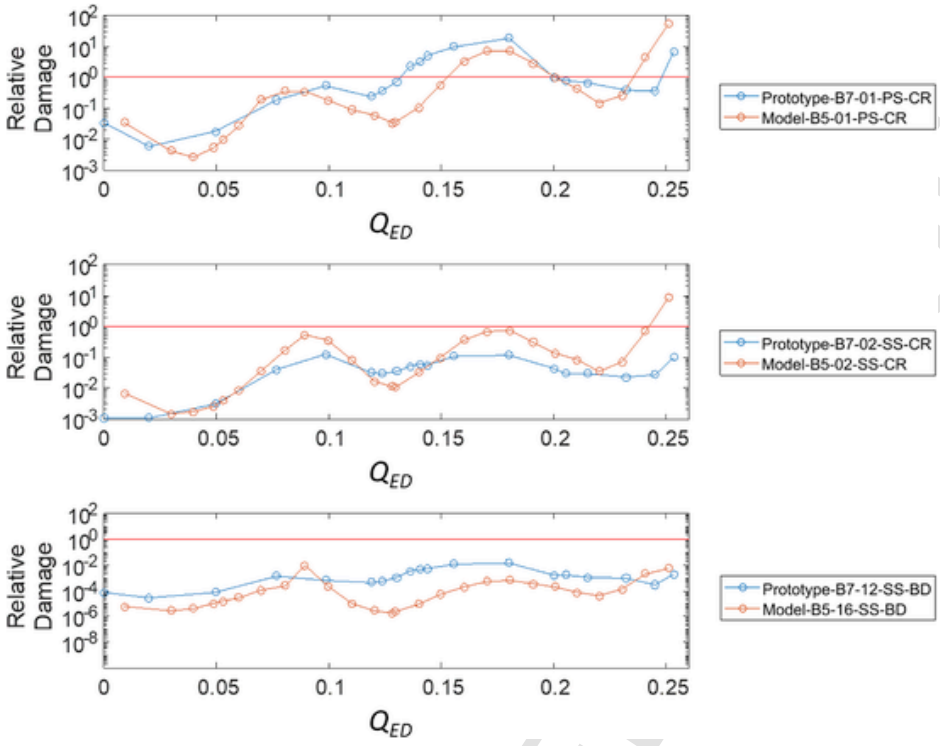

Fig. 9. Fatigue relative damage of all the operating conditions to the BEP.

ior has been confirmed by both model and prototype operations. These results permit to predict the stress distribution in the prototype by means of the ones in the model and therefore to avoid the most dangerous operating conditions for the runner while in operation.

The operation at deep part load ($Q_{ED} < 0.07$) presents the lower damage in terms of fatigue in the runner. However, at these operating conditions, interblade vortices can appear as [18,19] studied, inducing cavitation in the blade channels and producing erosive damage in the runner. Therefore, not only the fatigue damage (Fig. 9) has to be considered for the operation of the machine, but also the erosive cavitation that is not included in this work.

5. Mechanical transposition limitations

In this section, all the possibilities and limitations of the presented method for the mechanical transposition from model to prototype are listed.

From the modal behavior point of view, the parameters that can be transposed from model to prototype of the runner are the following:

- Natural frequencies: They are transposable in the air by applying the frequency scaling found in Table 5. However, in water they could not be transposable at all, since they depend on the nearby surfaces stiffness [36] and the surrounding water acoustical natural frequencies [37], parameters that are different in model and in prototype. Other parameters such as the seals clearance or the bearings stiffness, can affect also some natural frequencies of the runner and they are usually different in model and prototype.
- Mode-shapes: In air, they are the same in model and prototype. In water, since the parameters commented for the natural frequencies can be different between model and prototype, some mode-shapes could also be affected.
- Damping ratios: Not transposable in air. In water, the damping is dominated by the hydrodynamic damping [57] and there is not any evidence that the hydrodynamic damping can be transposed from model to prototype.

For the mechanical stress transposition, the points to take into account are listed below:

- The stress is transposable by using the relationship with the force applied to the structure. The scale to transpose stress from model to prototype is dependent on the specific energy scale and the pressure coefficient scale.
- The stress is transposable from model to prototype in the same location than the strain gauge is located in the model. The runner structure should be as similar as possible in model and prototype to not have different stiffness, especially in the blades.
- The stress is only transposable from model to prototype out of mechanical resonance conditions. In resonance conditions the amplitude is higher and cannot be predicted by the model.

Finally, according to the fatigue life estimation:

- Relative damage factors to one operating conditions are directly transposable from model to prototype as long as all the previous requirements for stress transposition are met.
- The stress time signal of the model has to be scaled by using the reduced frequency relationship between model and prototype in order to ensure that the frequencies included in the time signal are in the prototype scale.

6. Conclusions

A mechanical transposition method from model to prototype for Francis turbine runners is used, analyzed and compared in the present paper. To do so, mechanical similarity laws have been used and adapted to the hydraulic dimensionless parameters used for Francis turbines model testing. A prototype Francis turbine of 444 MW rated power and its analogous reduced scale (1:16) model have been used for study. Modal behavior, stress under operation and fatigue life-time pre-

dictions have been compared for both model and prototype. Results show the procedure to follow when transposing the mechanical behavior from model to prototype as well as the limitations of the method.

Natural frequencies, mode-shapes and damping ratios have been obtained experimentally in both model and prototype runners. Both runners were impacted in the air and its response was measured with accelerometers and strain gauges. Results show that the natural frequencies and mode-shapes are transposable by following the similarity laws presented in the paper, but the damping it is not. This means that the mechanical behavior of the runner is only transposable out of resonance conditions.

The runner stress under operation was measured in both model and prototype by using strain gauges located in different blades. Mean values and peak to peak values for the different operating conditions as well as frequency spectra of the strain gauges have been compared for both model and prototype. Results obtained show that the trend between the different strain gauges and for the different operating conditions is very similar in the model and in the prototype out of resonance conditions. A resonance between the third blade passing frequency and a runner natural frequency is found at certain operating conditions in the prototype but not in the model. This is happening because the excitation frequency is scaled from model to prototype by the runner rotating speed while the runner natural frequencies are scaled by the runner geometry.

The good agreement from model to prototype of the stress between operating conditions have permitted to compare the relative damage between operating conditions and also between different points of the blade. Rainflow counting algorithm have been used with the strain gauges signals of both model and prototype. The model signals were previously transposed to the prototype scale to be comparable. Results present very similar relative fatigue behavior for model and prototype, with some difference in the points where a natural frequency of the runner was excited in the prototype and not in the runner.

The method and results presented in this paper permit to use the stress obtained with reduced scale models to predict the stress and relative damage due to fatigue in the prototype. This is very helpful to see which operating conditions are worse for the runner and therefore operate the prototype Francis turbine according to this information. This could extend the useful life time of the runner at the same time than providing flexibility to the electrical grid.

Acknowledgements

The authors would like to acknowledge HYPERBOLE research project, granted by the European Commission (ERC/FP7-ENERGY-2013-1-Grant 608532). We also would like to acknowledge the “Ministerio de Eduación, Cultura y Deporte” together with “Campus de Excelencia International” for the international mobility scholarship (J-02096).

The authors would also like to thank BC Hydro for making possible the experimental tests in the prototype, Voith team for the strain gauges installation in the model and prototype, GE team for the pressure sensors installation in the prototype and the whole team of LMH (Laboratory for Hydraulic Machines) for performing the tests in the reduced scale model.

References

[1] A. Müller, A. Favrel, C. Landry, F. Avellan, Fluid–structure interaction mechanisms leading to dangerous power swings in Francis turbines at full load, J. Fluid Struct. 69 (2017) 56–71, doi:10.1016/j.jfluidstructs.2016.11.018.

[2] C. Bélanger, L. Gagnon, Adding wind energy to hydropower, Energy Pol. 30 (2002) 1279–1284, doi:10.1016/S0301-4215(02)00089-7.

[3] L. Gaudard, F. Romerio, The future of hydropower in Europe: interconnecting climate, markets and policies, Environ. Sci. Pol. 37 (2014) 172–181, doi:10.1016/j.envsci.2013.09.008.

[4] C. Valero, M. Egusquiza, E. Egusquiza, A. Presas, D. Valentin, M. Bossio, Extension of Operating Range in Pump-Turbines. Influence of Head and Load, Energies (2017), doi:10.3390/en10122178.

[5] A. Favrel, A. Müller, C. Landry, K. Yamamoto, F. Avellan, Study of the vortex-induced pressure excitation source in a Francis turbine draft tube by particle image velocimetry, Exp. Fluid 56 (2015) 215.

[6] A. Favrel, A. Müller, C. Landry, J. Gomes, K. Yamamoto, F. Avellan, Dynamics of the precessing vortex rope and its interaction with the system at Francis turbines part load operating conditions, Hyperbole Conf. Porto, Port. Febr., vols. 2–3, 2017, doi:10.1088/1742-6596/813/1/012023.

[7] A. Favrel, A. Müller, C. Landry, K. Yamamoto, F. Avellan, LDV survey of cavitation and resonance effect on the precessing vortex rope dynamics in the draft tube of Francis turbines, Exp. Fluid 57 (2016) 168, doi:10.1007/s00348-016-2257-y.

[8] A. Favrel, J.G.P. Junior, C. Landry, A. Müller, K. Yamaishi, F. Avellan, Dynamic modal analysis during reduced scale model tests of hydraulic turbines for hydro-acoustic characterization of cavitation flows, Mech. Syst. Signal Process. 117 (2019) 81–96, doi:10.1016/j.ymssp.2018.07.053.

[9] A. Presas, D. Valentin, E. Egusquiza, C. Valero, Detection and analysis of part load and full load instabilities in a real Francis turbine prototype, J. Phys. Conf. Ser. (2017), doi:10.1088/1742-6596/813/1/012038.

[10] D. Valentín, A. Presas, E. Egusquiza, C. Valero, M. Egusquiza, M. Bossio, Power swing generated in francis turbines by Part Load and overload instabilities, Energies 10 (2017) 2124.

[11] X. Escaler, E. Egusquiza, M. Farhat, F. Avellan, M. Coussirat, Detection of cavitation in hydraulic turbines, Mech. Syst. Signal Process. 20 (2006) 983–1007, doi:10.1016/j.ymssp.2004.08.006.

[12] D. Valentín, A. Presas, M. Egusquiza, C. Valero, E. Egusquiza, Transmission of high frequency vibrations in rotating systems. Application to cavitation detection in hydraulic turbines, Appl. Sci. 8 (2018), doi:10.3390/app8030451.

[13] E. Egusquiza, C. Valero, X. Huang, E. Jou, A. Guardo, C. Rodriguez, Failure investigation of a large pump-turbine runner, Eng. Fail. Anal. 23 (2012) 27–34, doi:10.1016/j.engfailanal.2012.01.012.

[14] C. Trivedi, A review on fluid structure interaction in hydraulic turbines: a focus on hydrodynamic damping, Eng. Fail. Anal. (2017).

[15] E. Egusquiza, C. Valero, A. Presas, X. Huang, A. Guardo, U. Seidel, Analysis of the dynamic response of pump-turbine impellers. Influence of the rotor, Mech. Syst. Signal Process. (2016) 68–69 330–341, doi:10.1016/j.ymssp.2015.05.034.

[16] W.J. Rheingans, Power swings in hydroelectric power plants, Trans. ASME. 62 (1940) 171–184.

[17] I.E. Commission, Hydraulic Turbines, Storage Pumps and Pump-Turbines |model Acceptance Tests, Standard No. IEC 60193, 1999.

[18] K. Yamamoto, A. Müller, A. Favrel, F. Avellan, Experimental evidence of inter-blade cavitation vortex development in Francis turbines at deep part load condition, Exp. Fluid 58 (2017) 142, doi:10.1007/s00348-017-2421-z.

[19] K. Yamamoto, A. Müller, A. Favrel, C. Landry, F. Avellan, Flow characteristics and influence associated with inter-blade cavitation vortices at deep part load operations of a Francis turbine, Hyperbole Conf. Porto, Port. Febr., vols. 2–3, 2017, doi:10.1088/1742-6596/813/1/012029.

[20] Z. Zhang, Y. Wang, Z. Fan, Similarity analysis between scale model and prototype of large vibrating screen, Shock Vib. 2015 (2015).

[21] A. Jha, R. Sedaghati, R. Bhat, Dynamic testing of structures using scale models, 46th AIAA/ASME/ASCE/AHS/ASC Struct. Struct. Dyn. Mater. Conf., 2005, p. 2259.

[22] C.D. Norman, H.E. Stone, Comparison of Vibration Test Results for a Model and Prototype Gravity Dam, 1981.

[23] H. Tanaka, Vibration behavior and dynamic stress of runners of very high head reversible pump-turbines, Int. J. Fluid Mach. Syst. 4 (2011) 289–306.

[24] R.D. Blevins, Formulas for Natural Frequency and Mode Shape, Krieger Publishing Company, 2001. http://books.google.es/books?id=ee1_AAAACAAJ.

[25] D. Valentín, A. Presas, E. Egusquiza, C. Valero, Experimental study on the added mass and damping of a disk submerged in a partially fluid-filled tank with small radial confinement, J. Fluid Struct. 50 (2014) 1–17, doi:10.1016/j.jfluidstructs.2014.06.006.

[26] F. Alijani, M. Amabili, P. Balasubramanian, S. Carra, G. Ferrari, R. Garziera, Damping for large-amplitude vibrations of plates and curved panels, Part 1: modeling and experiments, Int. J. Non Lin. Mech. 85 (2016) 23–40.

[27] A. Presas, D. Valentin, E. Egusquiza, C. Valero, M. Egusquiza, M. Bossio, Accurate determination of the frequency response function of submerged and confined structures by using PZT-patches, Sensors (2017) 17, doi:10.3390/s17030660.

[28] A. Presas, E. Egusquiza, C. Valero, D. Valentin, U. Seidel, Feasibility of Using PZT Actuators to Study the Dynamic Behavior of a Rotating Disk Due to Rotor-Stator Interaction, Sensors (2014), doi:10.3390/s140711919.

[29] C.G. Rodriguez, E. Egusquiza, X. Escaler, Q.W. Liang, F. Avellan, Experimental investigation of added mass effects on a Francis turbine runner in still water, J. Fluid Struct. 22 (2006) 699–712, doi:10.1016/j.jfluidstructs.2006.04.001.

[30] Q.W. Liang, C.G. Rodríguez, E. Egusquiza, X. Escaler, M. Farhat, F. Avellan, Numerical simulation of fluid added mass effect on a francis turbine runner, Comput. Fluids 36 (2007) 1106–1118, doi:10.1016/j.compfluid.2006.08.007.

[31] D. Valentín, D. Ramos, M. Bossio, A. Presas, E. Egusquiza, C. Valero, Influence of the boundary conditions on the natural frequencies of a Francis turbine, 28th IAHR Symp, Hydraul. Mach. Syst., 2016, doi:10.1088/1755-1315/49/7/072004.

[32] A. Presas, D. Valentin, E. Egusquiza, C. Valero, U. Seidel, Dynamic response of a rotating disk submerged and confined. Influence of the axial gap, J. Fluid Struct. (2016), doi:10.1016/j.jfluidstructs.2016.02.003.

[33] A. Presas, D. Valentin, E. Egusquiza, C. Valero, U. Seidel, Influence of the rotation on the natural frequencies of a submerged-confined disk in water, J. Sound Vib. 337 (2015) 161–180, doi:10.1016/j.jsv.2014.10.032.

[34] A. Presas, D. Valentin, E. Egusquiza, C. Valero, U. Seidel, On the detection of natural frequencies and mode shapes of submerged rotating disk-like struc-

tures from the casing, Mech. Syst. Signal Process. 60 (2015) 547–570, doi:10.1016/j.ymssp.2015.01.013.
[35] D. Valentín, A. Presas, E. Egusquiza, C. Valero, On the capability of structural–acoustical fluid–structure interaction simulations to predict natural frequencies of rotating disklike structures submerged in a heavy fluid, J. Vib. Acoust. 138 (2016) 34502, doi:10.1115/1.4032726.
[36] D. Valentín, A. Presas, E. Egusquiza, C. Valero, M. Egusquiza, Experimental study of a vibrating disk submerged in a fluid-filled tank and confined with a nonrigid cover, J. Vib. Acoust. 139 (2017) 21005.
[37] M. Bossio, D. Valentín, A. Presas, D.R. Martin, E. Egusquiza, C. Valero, M. Egusquiza, Numerical study on the influence of acoustic natural frequencies on the dynamic behaviour of submerged and confined disk-like structures, J. Fluid Struct. 73 (2017) 53–69, doi:10.1016/j.jfluidstructs.2017.05.008.
[38] X. Liu, Y. Luo, Z. Wang, A review on fatigue damage mechanism in hydro turbines, Renew. Sustain. Energy Rev. 54 (2016) 1–14.
[39] X. Huang, J. Chamberland-Lauzon, C. Oram, A. Klopfer, N. Ruchonnet, Fatigue analyses of the prototype Francis runners based on site measurements and simulations, 27th IAHR Symp. Hydraul. Mach. Syst., 2014, doi:10.1088/1755-1315/22/1/012014.
[40] M. Gagnon, S.A. Tahan, P. Bocher, D. Thibault, Impact of startup scheme on Francis runner life expectancy, 25th IAHR Symp, Hydraul. Mach. Syst., 2010, doi:10.1088/1755-1315/12/1/012107.
[41] B. Nennemann, J.F. Morissette, J. Chamberland-Lauzon, C. Monette, O. Braun, M. Melot, A. Coutu, J. Nicolle, A.M. Giroux, Challenges in dynamic pressure and stress predictions at No-load operation in hydraulic turbines, 27th IAHR Symp, Hydraul. Mach. Syst., 2014, doi:10.1088/1755-1315/22/3/032055.
[42] D. Valentín, A. Presas, M. Bossio, M. Egusquiza, E. Egusquiza, C. Valero, Feasibility of detecting natural frequencies of hydraulic turbines while in operation, using strain gauges, Sensors 18 (2018) 174.
[43] U. Seidel, C. Mende, B. Hübner, W. Weber, A. Otto, Dynamic loads in Francis runners and their impact on fatigue life, 27th IAHR Symp, Hydraul. Mach. Syst., 2014, doi:10.1088/1755-1315/22/3/032054.
[44] F. Duparchy, J. Brammer, M. Thibaud, A. Favrel, P.Y. Lowys, F. Avellan, Mechanical impact of dynamic phenomena in Francis turbines at off design conditions, J. Phys. Conf. Ser., 2017, p. 12035.
[45] F. Duparchy, A. Favrel, P.Y. Lowys, C. Landry, A. Müller, K. Yamamoto, F. Avellan, Analysis of the part load helical vortex rope of a Francis turbine using on-board sensors, 9th Int. Symp. Cavitation Lausanne, Switz., 2015, doi:10.1088/1742-6596/656/1/012061.
[46] C.G. Rodriguez, E. Egusquiza, I.F. Santos, Frequencies in the vibration induced by the rotor stator interaction in a centrifugal pump turbine, J. Fluid Eng. 129 (2007) 1428–1435, doi:10.1115/1.2786489.
[47] A. Presas, E. Egusquiza, C. Valero, D. Valentin, U. Seidel, Feasibility of using PZT actuators to study the dynamic behavior of a rotating disk due to rotor-stator interaction, Sensors 14 (2014) 11919–11942, doi:10.3390/s140711919.
[48] N. Ruchonnet, C. Nicolet, F. Avellan, One-dimensional modeling of rotor stator interaction in Francis pump-turbine, Proc. 23rd IAHR Symp. Hydraul, Mach. Syst., 2006.
[49] D. Valentín, A. Presas, E. Egusquiza, C. Valero, M. Egusquiza, M. Bossio, Power swing generated in francis turbines by Part Load and overload instabilities, Energies (2017), doi:10.3390/en10122124.
[50] Hyperbole Project, HYdropower Plants PERformance and flexiBle Operation towards Lean Integration of New Renewable Energies, 2013. https://hyperbole.epfl.ch.
[51] D. Valentin, A. Presas, M. Bossio, M. Egusquiza, E. Egusquiza, C. Valero, Feasibility to detect natural frequencies of hydraulic turbines under operation using strain gauges, Proceedings (2017), doi:10.3390/proceedings1080821.
[52] E. Egusquiza, D. Valentín, A. Presas, C. Valero, Overview of the experimental tests in prototype, J. Phys. Conf. Ser. (2017), doi:10.1088/1742-6596/813/1/012037.
[53] A. Presas, D. Valentin, M. Egusquiza, C. Valero, E. Egusquiza, A. Presas, D. Valentin, M. Egusquiza, C. Valero, E. Egusquiza, Sensor-based optimized control of the full load instability in large hydraulic turbines, Sensors 18 (2018) 1038, doi:10.3390/s18041038.
[54] M. Binda, T. Harčarik, F. Šimčák, Modal parameters estimation by using PULSE Reflex modal analysis, 4th Int. Conf. Model. Mech. Mechatron. Syst., Faculty o f Mechanical Engineering,Technical University of Košice, 2011, pp. 17–21.
[55] C. Trivedi, Compressible large eddy simulation of a francis turbine during speed-No-load: rotor stator interaction and inception of a vortical flow, J. Eng. Gas Turbines Power 140 (2018) 112601–112618, doi:10.1115/1.4039423.
[56] S.D. Downing, D.F. Socie, Simple rainflow counting algorithms, Int. J. Fatig. 4 (1982) 31–40, doi:10.1016/0142-1123(82)90018-4.
[57] J.P. Gauthier, A.M. Giroux, S. Etienne, F.P. Gosselin, A numerical method for the determination of flow-induced damping in hydroelectric turbines, J. Fluid Struct. 69 (2017) 341–354, doi:10.1016/j.jfluidstructs.2017.01.004.

Nomenclature

Acronyms

BEP: :Best Efficiency Point
EMA: :Experimental Modal Analysis
RSI: :Rotor Stator Interaction
VR: :Vortex Rope
FRF: :Frequency Response Function
ODS: :Operational Deflection Shape
CMIF: :Complex Mode Indication Function
NPSE: :Net Positive Suction Energy

Subscripts

M: :Model
P: :Prototype
n: :Net
r: :Reduced
b: :Blade
v: :Guide vane
i: :Integer number (1,2, …,∞)
j: :Integer number (1,2, …,∞)
m: :Mass
c: :Damping
k: :Stiffness
ρ: :Density
Y: :Elasticity
L: :Characteristic length
ω: :Natural frequency
ξ: :Damping ratio
ψ: :Mode-shape
F: :Force
E: :Specific speed
σ: :Stress
CP: :Pressure coefficient

Dimensionless numbers

$Re = \frac{vL}{\nu}$: :Reynolds
$Eu = \frac{\Delta P}{\rho v^2}$: :Euler
$Fr = \frac{v}{\sqrt{gL}}$: :Froude
$We = \frac{\rho L v^2}{\gamma}$: :Weber
$St = \frac{fL}{v}$: :Strouhal
$\sigma_{thoma} = \frac{NPSE}{E}$: :Thoma number
$n_{ED} = \frac{nD}{E^{0.5}}$: :Speed factor
$Q_{ED} = \frac{Q}{D^2 E^{0.5}}$: :Discharge factor
$Cp = \frac{\Delta p}{\rho E}$: :Pressure coefficient
$F_{ED} = \frac{F}{\rho D^2 E}$: :Force factor
$\pi_1 = \frac{F}{L^2 Y_\varepsilon}$: :Hooke's law dimensionless number
$\pi_2 = \frac{FF}{\rho L^4}$: :Newton's second law dimensionless number
$\pi_3 = \frac{F\sqrt{c}}{l_c^2}$: :Internal friction law dimensionless number
$\lambda_m = \lambda_L^3 \lambda_\rho$: :Modal Mass Scale
$\lambda_c = \lambda_L^2 \sqrt{\lambda_\rho \lambda_Y}$: :Modal Damping Scale
$\lambda_k = \lambda_L \lambda_Y$: :Modal Stiffness Scale
$\lambda_\omega = \frac{1}{\lambda_L}\sqrt{\frac{\lambda_\rho}{\lambda_Y}}$: :Frequency Scale
$\lambda_\xi = 1$: :Damping ratio Scale
$\lambda_\psi = 1$: :Mode Shape Scale

Variables

v: :Velocity ($m \cdot s^{-1}$)
L: :Characteristic length (m)
P: :Pressure (Pa)
g: :Gravity ($m \cdot s^{-2}$)
E: :Specific energy (J/kg)
n: :Runner rotating frequency (Hz)
D: :Outlet diameter of the runner (m)
Q: :Discharge ($m^3 \cdot s$)
F: :Force (N)
f: :Frequency
H: :Head (m)
z: :Number of blades (b) or guide vanes (v)
$k_{i,j}$: :Shape of the pressure distribution
Y: :Young modulus (Pa)
t: :Time (s)
C: :Damping coefficient ($N \cdot s \cdot m^{-1}$)
M: :Mass (kg)
K: :Stiffness (N/m)
u: :Displacement (m)

Greek letters

λ: :Scale (dimensionless)
ν: :Kinematic viscosity ($m^2 \cdot s$)
ρ: :Density ($kg \cdot m^{-3}$)
γ: :Surface tensions (N/m)
ε: :Strain (m/m)
ξ: :Damping ratio (%)
ψ: :Mode shape
ω: :Angular frequency (rad/s)
σ: :Stress (Pa)
β: :Internal damping constant ($m^4 \cdot N^{-2}$)